Spectral Decomposition Method for Large Sea Surface Generation and Radar Backscatter Modeling

Aymeric Mainvis, Vincent Fabbro, Christophe Bourlier, Henri-Jose Mametsa

Spectral Decomposition Method for Large Sea Surface Generation and Radar Backscattering

Aymeric Mainvis, Vincent Fabbro, Christophe Bourlier and Henri-Jose Mametsa

Abstract

This paper presents an original method to simulate rapidly a realization of a large sea surface and also investigates its impact on the backscattering normalized radar cross section (BNRCS). Indeed, for radar microwaves frequencies an for wind speed between 1 and 10 m/s the area of the sea surfaces must be ranged from 50 to 200 m^2 to take into account all the surface roughness scales, which can contribute to the scattering process. The proposed method consists in splitting up the full sea surface height spectrum into sub-spectra of smaller scales and recombining the resulting sea height generations from different interpolations and recombination techniques. A closed-form expression of the resulting sea surface height spectrum is also derived to interpret the simulation results. Finally, from the first-order Small Slope Approximation (SSA1) scattering model, the BNRCS computed from sea surfaces generated by the suggested method and the conventional method are compared to show the efficiency of the method in terms of accuracy and memory consumption.

Index Terms

Sea surface, spectral method, small slope approximation, radar scattering, ocean remote sensing.

I. Introduction

Deterministic model –and sea surface generation in particular– is a key-element within the radar sensor design optimization but also within the modeling and understanding chain of measurements. Either from airborne or satellite sensors or from satellite ones, sea surface generation makes it possible to compute the radar backscattering and therefore, to investigate the recorded data, like altimeters data. However, some radar systems (like satellite Synthetic Aperture Radar) require a sea surface generation with large area and high resolution. So, it becomes crucial to offer low-consumption sea surface generation model in terms of computing resources and / or time requirement. Indeed, electromagnetic (EM) wave scattering from random rough surfaces models –like the first-order Small Slope Approximation (SSA1) method [1]– require a small surface sampling interval to obtain accurate results. Commonly, for convergence criteria, this sampling interval is equal to one-tenth of the incident radar wavelength. Furthermore, a large scale of waves within the sea surface have to be taken correctly into account to simulate the sea surface geometry. In particular, the gravity and gravity-capillary waves drive the EM scattering from the illuminated sea surface and so constrain the sea surface area. Therefore, EM scattering of large sea surfaces remains a critical computing constraint.

A fast simulation of a sea surface is described in [2]. Pinel et al. studied the slope probability density function and the slope autocorrelation function after dividing the height sea spectrum in two parts and generating sea surfaces with different spatial resolutions. In [3], Jiang et al. introduced the spectral decomposition method to reduce memory consumption and generate different-scale rough surfaces. The whole spectrum is divided in several parts used to generate these different-scale rough surfaces. This method is applied to perform unified device architecture (CUDA) parallel computation. This approach and the conventional one are tested and compared with the first-order SSA1. The same method is then studied for sea surface generation in [4] and tested with SSA1 by simulating the sea surface backscattering normalized radar cross section (BNRCS) and Doppler spectra. This paper provides a quantitative analysis of the spectral decomposition method. Indeed, this particular sea surface generation is analytically described and developed to express its computational complexity and its memory consumption. Furthermore, an in depth study is also performed to highlight the impact of the interpolation process and the two suggested combination techniques on the sea surface characteristics and on the BNRCS.

Section II details the formalism of the spectral decomposition method which describes a split-spectrum process and a reconstructed sea surface generation with an interpolated surface and a combination technique. Section III introduces the SSA1 method and the sea surface BNRCS expression. Section IV presents numerical results for a two-dimensional problem by evaluating the sea surface height spectrum and the height structure function. BNRCS computed from SSA method considering a conventional sea surface generation and the Spectral Decomposition Method (SDM) are described in Section V. The influence of SDM parameters are discussed.

II. Sea Surface Generation and Spectral Decomposition Method

A. Sea Surface Model

From a conventional spectral method, the height of sea surface $H(\mathbf{r},t)$ is expressed as [5]

$$H(\mathbf{r},t) = \mathrm{Re}\left[\int_{\mathbb{R}^2} \sqrt{S(\mathbf{k})}E(\mathbf{k})e^{-j\omega(\mathbf{k})t}e^{j\mathbf{k}\cdot\mathbf{r}}d\mathbf{k}\right], \tag{1}$$

where $\mathbf{r}=\mathbf{r}(x,y)$ the Cartesian position, t the time, $S(\mathbf{k})$ the height sea spectrum, $\mathbf{k}$ the wavenumber vector, E a gaussian process and $\omega(\mathbf{k})$ the pulsation defined through a dispersion relation [6]. This conventional method is very efficient for sea surface generation, allowing to use Fast Fourier Transform (FFT). However, EM scattering computation using rigorous techniques requires an accurate sampling of the surface, inducing prohibitive computing ressources for high frequency and for high sea state in a three-dimensional problem. For this reason an optimization of the method is proposed by applying a spectral decomposition.

B. Spectral Decomposition Method

To introduce the Spectral Decomposition Method; first, the function Γ is defined as

$$\Gamma(\mathbf{k},t) = \sqrt{S(\mathbf{k})}E(\mathbf{k})e^{-j\omega(\mathbf{k})t}. \tag{2}$$

Then, this function is split up into N functions Γ_n such as

$$\Gamma_n(\mathbf{k},t) = \begin{cases} \Gamma(\mathbf{k},t) & \text{if } k_n \leq \|\mathbf{k}\| < k_{n+1} \\ 0 & \text{else,} \end{cases} \tag{3}$$

with Γ defined in Eq. (2), $\mathbf{k}$ the wavenumber vector, k_n the cutoff-wavenumber, for which $k_0 = 0$, $k_N = +\infty$ and $n \in [0, N-1]$. Consequently, one has to choose $N-1$ cutoff-wavenumbers k_n to define Γ_n. Eq. (1) can be rewritten as

$$\begin{aligned} H(\mathbf{r},t) &= \mathrm{Re}\left[\sum_{n=0}^{N-1}\int_{\|\mathbf{k}\|=k_n}^{\|\mathbf{k}\|<k_{n+1}} \Gamma(\mathbf{k},t)e^{j\mathbf{k}\cdot\mathbf{r}}d\mathbf{k}\right] \\ &= \mathrm{Re}\left[\sum_{n=0}^{N-1}\int_{\mathbb{R}^2} \Gamma_n(\mathbf{k},t)e^{j\mathbf{k}\cdot\mathbf{r}}d\mathbf{k}\right] \\ &= \mathrm{Re}\left[\sum_{n=0}^{N-1} h_n(\mathbf{r},t)\right], \end{aligned} \tag{4}$$

with $h_n(\mathbf{r},t)$ the height of sea surface generated from the n-th part Γ_n. Here, the full generated sea surface $H(\mathbf{r},t)$ is seen as the summation of N elementary generated sea surfaces, corresponding to a specific roughness scale.

C. Reconstructed Sea Surface

Computing sea surface implies choosing a surface size $L_x \times L_y$ (or $N_x \times N_y$ sampling points) and sampling intervals (Δ_x, Δ_y). For more clarity, the surface length and the sampling interval to generate the sea surface H are chosen such as $L_x = L_y = L_0$ and $\Delta_x = \Delta_y = \Delta$, respectively. Then, by applying SDM and from Eq. (3), the use of FFT to generate each surface –corresponding to the different roughness scales– implies

$$k_n = \frac{2\pi}{L_n} \qquad k_0 = \frac{2\pi}{L_0} \qquad k_N = \frac{\pi}{\Delta}, \tag{5}$$

with $n \in [0, N-1]$, $L_n = N_n \times \Delta_n$ the length of the sea surface h_n linked to the cutoff-wavenumber k_n in Eq. (4) with N_n sampling points and Δ_n the sampling interval. So, selecting cutoff-wavenumber k_n in SDM leads to the parameters of h_n

$$L_n = \frac{2\pi}{k_n} \qquad \Delta_n = \frac{2\pi}{N_n k_n}. \tag{6}$$

Eq. (3) and (6) imply

$$L_n > L_{n+1}, \tag{7}$$

and Eq. (6) leads to

$$\Delta_n > \Delta_{n+1}, \tag{8}$$

if $N_n = N$, a constant. Consequently, generating sea surfaces by using SDM induces a sea surfaces serie, each sea surface with different sizes and different sampling intervals. However, to be able to sum the different surfaces corresponding to the different roughness scales, the surface meshings must be equal. Then, to solve this problem, two techniques are suggested: an interpolation process and a combination technique. Fig. 1 plots a schematic diagram for the generation of surfaces h_n and h_{n+1} and their respective length, L_n and L_{n+1}, and sampling interval, Δ_n and Δ_{n+1} according to the SDM. The interpolation process is a way to reduce the sampling interval from Δ_n to Δ, the smallest sampling interval. In this paper, three kinds of interpolation are studied, namely, linear, quadratic and cubic. The combination technique is a way to increase the surface length from L_n to L_0, the largest surface length. For example, the interpolation process is a mean to get the same size between the two sea surfaces in

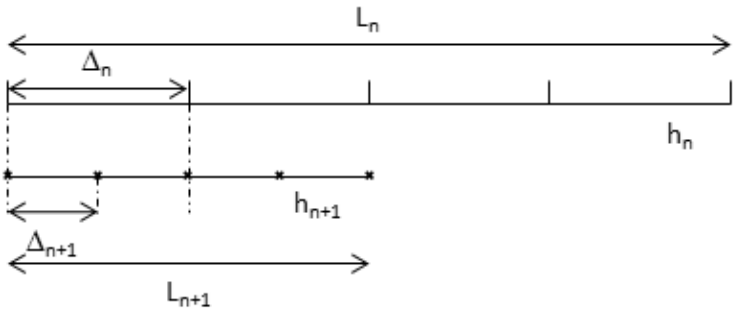

Fig. 1. Schematic diagram for the generation of surfaces h_n and h_{n+1} according to the Spectral Decomposition Method.

Fig. 1 and the combination technique, the mean to get the same sampling interval. Thus, these two surfaces can be finally additionated. For a sake of clarity, a focus on a two-dimensional problem and a spectrum division into two parts is proposed to formalize the combination techniques. Thus, the total sea surface H is composed of a low-frequencies-scale sea surface h_{LF} and a high-frequencies-scale one h_{HF}

$$H(x) = h_{\text{LF}}(x) + h_{\text{HF}}(x), \tag{9}$$

h_{LF} is the interpolated sea surface and h_{HF} the combined one. Two combination techniques are studied: the Repeated Surfaces Technique (RST) and the Combined Surfaces Technique (CST). Then, the RST principle is that the final HF surface is composed of P times the same HF surface. It can be formalized by

$$h_{\text{HF,RST}}(x) = h_{\text{HF}}(x) * \sum_{n=0}^{P-1} \delta(x - nL), \tag{10}$$

with $*$ the product-convolution operator, h_{HF} the P-times-repeated surface, L its length, $h_{\text{HF,RST}}$ the composed surface of length $P \times L$ and δ the Dirac delta function. This combination technique ensures the continuity between each combined surface h_{HF} thanks to the FFT property. The CST is defined by Jeannin et al. [7], a composite surface h_{comp} is defined by

$$h_{\text{comp}}(x) = \frac{\sqrt{d-x}h_1(x+L-d) + \sqrt{x}h_2(x)}{\sqrt{d}}, \tag{11}$$

with $x \in [0; d]$, h_1 and h_2 two independent rough surfaces with length L. These two surfaces are combined on an interval d. Then,

$$h_{\text{HF,CST}}(x) = \sum_{n=0}^{P-1} h_{\text{HF,int},n}(x) * \delta[x - n(L-d)], \tag{12}$$

with

$$h_{\text{HF,int},n}(x) = \begin{cases} h_{\text{HF,comp},n-1}(x) & \text{if } x \in [0; d] \\ h_{\text{HF},n}(x) & \text{if } x \in]d; L-d], \end{cases} \tag{13}$$

and $h_{\text{HF},n}$ the rough surface generated from a unique random gaussian process and

$$h_{\text{HF,comp},n}(x) = \frac{\sqrt{d-x}h_{\text{HF},n}(x+L-d) + \sqrt{x}h_{\text{HF},n+1}(x)}{\sqrt{d}}. \tag{14}$$

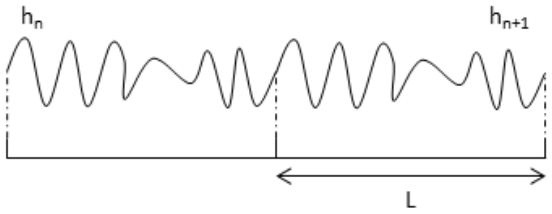

(a) Repeated Surfaces Technique

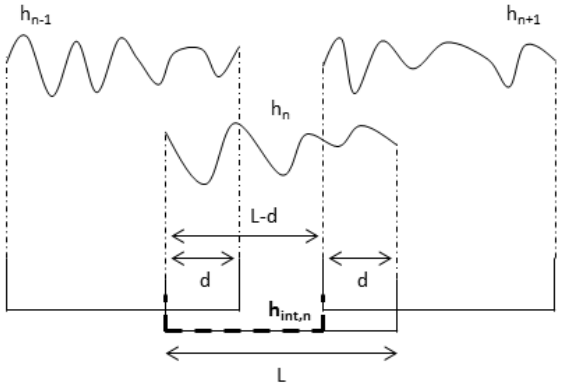

(b) Combined Surfaces Technique

Fig. 2. Schematic diagram for the generation of surface h_{HF} with any of the two combination techniques, RST (2a) and CST (2b).

Thus $h_{\text{HF,int},n}$ is a rough surface of length $(L-d)$. Furthermore,

$$h_{\text{HF,comp},-1}(x) = \frac{\sqrt{d-x}h_{P-1}(x+L-d) + \sqrt{x}h_0(x)}{\sqrt{d}}, \tag{15}$$

to ensure the combined sea surface periodicity and so, the continuity. The composed surface $h_{\text{HF,CST}}$ length is equal to $(L-d)P$. This technique keeps continuity between each combined surface $h_{\text{HF,int},n}$. For a simplicity reason, the interval d is chosen as $L/2$ in this work. Fig. 2 illustrates a schematic diagram for the generation of the surface h_{HF} with any of the two combination techniques, RST (2a) and CST (2b). To check the sea spectrum integrity, the HF sea height spectrum from RST is expressed. It can be written as

$$S_{\text{HF,RST}}(k) = \frac{S_{\text{HF}}(k)}{P}\left|\frac{\sin\left(\frac{kPL}{2}\right)}{\sin\left(\frac{kL}{2}\right)}\right|^2 \tag{16}$$

with $S_{\text{HF,RST}}$ the spectrum from RST, S_{HF} the sea height spectrum used to generate the P combined surfaces of length L and k the wavenumber. The proof is detailed in Appendix A. Then, from Eq. (16), it appears that $S_{\text{HF,RST}}$ is the conventional sea spectrum S_{HF} modulated by a $2\pi/L$-periodic function. This function has local maxima for

$$\frac{kL}{2} = n\pi \Leftrightarrow k = \frac{n2\pi}{L}, \tag{17}$$

with $n \in \mathbb{Z}$. To quantify the efficiency of the SDM, the computational complexity of the FFT is a relevant tool. This is expressed as

$$\mathcal{O}(N\log_2 N), \tag{18}$$

with N the number of samples computed by FFT. Let us consider a simple 3D case, as previously discussed, the spectrum is divided into two parts like in Eq. (9), that is

$$H(\mathbf{r},t) = h_{\text{LF}}(\mathbf{r},t) + h_{\text{HF}}(\mathbf{r},t), \tag{19}$$

with h_{LF} the interpolated sea surface and h_{HF} the reconstructed one. According to the chosen combination technique, the computational complexity C_{HF} linked to the surface generation h_{HF} is

$$C_{\text{HF}} = \begin{cases} \mathcal{O}(N_{\text{HF}}^2 \log_2 N_{\text{HF}}^2) & \text{if RST} \\ \frac{L}{L-d} P \times \mathcal{O}(N_{\text{HF}}^2 \log_2 N_{\text{HF}}^2) & \text{if CST,} \end{cases} \tag{20}$$

with N_{HF}^2 the number of samples of each combined surface of area L^2, d the CST parameter in Eq. (12) and P the number of combined high-frequencies-scale surfaces. So, the computational complexity C_T to generate the sea surface H is

$$C_T = \mathcal{O}(N_{\text{LF}}^2 \log_2 N_{\text{LF}}^2) + C_{\text{HF}}, \tag{21}$$

with N_{LF}^2 the number of samples of h_{LF} before interpolation process. For example, suppose $N_{\text{LF}} = N_{\text{HF}} = N$, then,

$$C_T = (1+\alpha) \times \mathcal{O}(N^2 \log_2 N^2), \tag{22}$$

$\alpha = 1$ or $PL/(L-d)$ Eq. (20). The equivalent computational complexity C_{ref} for a conventional sea surface generation is

$$C_{\text{ref}} = \mathcal{O}(P^2 N^2 \log_2 P^2 N^2). \tag{23}$$

Indeed, with a given number of samples N^2 and a given sampling interval Δ, the total area of the generated sea surface thanks to SDM is $L^2 = (P \times N \times \Delta)^2$. So, by keeping the same sampling interval, $(N \times P)^2$ sampling points are needed to reach the same area. Fig. 3 sets out the computational complexity of sea surface generation versus the number of samples N with $P = 8$ according to Eq. (22) (RST and CST) and Eq. (23) (Reference). This result shows a gain between 5 and 14 (for a number of samples $N = 10^4$) by using SDM rather than a conventional sea surface generation. Fig. 4 plots the computational complexity of sea surface generation versus the number of combined surfaces P with $N = 2^{13}$. This time, the gain is between 10 (for CST) and 200 (for RST) by using SDM and considering a parameter $P = 16$. These simulations clearly highlight the interest of such a multiscale method. For memory consumption, by keeping the same notations introduced in Eq. (22) and Eq. (23), the total memory consumption to store generated sea surface data is

$$M_{\text{ref}} = m P^2 N^2 \tag{24}$$

$$M_T = m(1+\alpha) N^2, \tag{25}$$

with m the memory allocation of an elementary piece of data, M_{ref} the memory consumption for a conventional sea surface generation and M_T the one for SDM with $\alpha = 1$ for RST or $\alpha = PL/(L-d)$ for CST Eq. (20). According to Elfouhaily et al. [6], the minimum surface wavenumber $k_{\min}$ should verify $k_{\min} \approx 0.3 k_p$ with

$$k_p \approx \Omega^2 g / u_{10}^2, \tag{26}$$

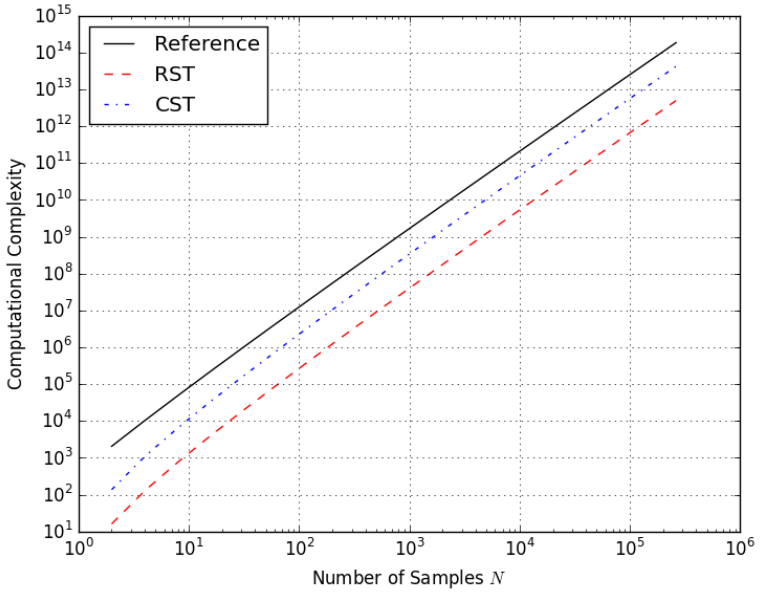

Fig. 3. Computational complexity of sea surface generation versus the number of samples N with $P=8$

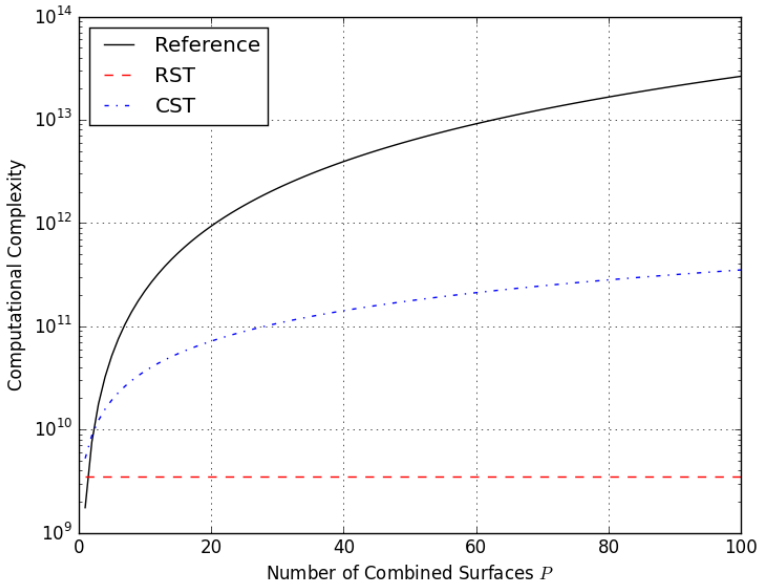

Fig. 4. Computational complexity of sea surface generation versus the number of combined surfaces P with $N=2^{13}$

where Ω is the inverse wave age equal to 0.84 in a case of a fully developed sea, g the acceleration of gravity and u_{10} the wind speed at ten meters above the sea. So, with a sampling interval of one-tenth of the incident radar wavelength and $u_{10}=8$ m/s; $67,108,864$ samples are needed to generate a conventional 3D sea surface. That is $536,870,912$ octets for a *float64* ($m=8$ octets). For SDM, with $\alpha=1$ for RST and $P=8$ combined surfaces, $M_T=16,777,216$ octets. The memory consumption ratio is $1/32$. Tab. I gives the memory consumption ratio

TABLE I
MEMORY CONSUMPTION RATIO

Number of combined surfaces	RST	CST
$P = 8$	0.031	0.266
$P = 16$	0.008	0.129
$P = 32$	0.002	0.064

M_T/M_{ref} versus the number of combined surfaces P and the combination technique. Once again, the SDM is more efficient than the conventional sea surface generation.

III. SIMULATED RADAR BACKSCATTERING

To analyze the impact of SDM on EM scattering, the BNRCS is considered, computed by a local model, the first-order Small Slope Approximation (SSA1).

First-Order Small Slope Approximation

The SSA1 is efficient in the whole range of incidence angles, from $0°$ (nadir) to $60°$. The scattering operator is given by [1]

$$\mathbb{S}(\mathbf{k},\mathbf{k_0}) = \frac{\mathbb{B}(\mathbf{k},\mathbf{k_0})}{Q_z}\int_{\mathbf{r}} e^{-jQ_z\eta(\mathbf{r})}e^{-j\mathbf{Q_H}\cdot\mathbf{r}}d\mathbf{r}, \tag{27}$$

with $\mathbb{B}(\mathbf{k},\mathbf{k_0})$ the first-order small perturbation model (SPM1) kernel [8], a polarization term, $\mathbf{Q_H}$ and Q_z horizontal and vertical components of the vector $\mathbf{Q}=\mathbf{k}-\mathbf{k_0}$, respectively, $\mathbf{k_0}$ and $\mathbf{k}$ the incidence and observation wave vectors and $\eta(\mathbf{r})$ the surface elevation. Then, the incoherent normalized radar cross section (NRCS) of an infinite surface σ_0 is expressed as

$$\sigma_0(\mathbf{k},\mathbf{k_0}) = \frac{\langle\mathbb{S}(\mathbf{k},\mathbf{k_0})\mathbb{S}^*(\mathbf{k},\mathbf{k_0})\rangle}{\kappa\Sigma} - \frac{\langle\mathbb{S}(\mathbf{k},\mathbf{k_0})\rangle\langle\mathbb{S}(\mathbf{k},\mathbf{k_0})\rangle^*}{\kappa\Sigma}, \tag{28}$$

with $\mathbb{S}(\mathbf{k},\mathbf{k_0})$ defined in Eq.(27), Σ the sea surface area (length in a 2D problem) and κ a constant equal to π for a 3D problem and $4k_0$ for a 2D problem with k_0 the radar wavenumber. In this numerical approach, a Thorsos beam [9] of parameter $g=L/3$ (with L the total length of the sea surface) is considered to illuminate the generated sea surface. This beam is a tapered plane wave with a Gaussian shape; the tapering is used to reduce the incident field to near zero at the ends of the generated sea surface and so, to reduce the potential edge effects to a negligible levels. From Eq. (28) and for a Gaussian process, an analytical expression of the incoherent NRCS [10] can also be performed,

$$\begin{aligned}\sigma_0(\mathbf{k},\mathbf{k_0}) &= \frac{|\mathbb{B}(\mathbf{k},\mathbf{k_0})|^2}{\kappa Q_z^2}e^{-Q_z^2\sigma_\eta^2}\int_{\mathbf{r}} e^{-j\mathbf{Q_H}\cdot\mathbf{r}}\left[e^{Q_z^2W(\mathbf{r})}-1\right]d\mathbf{r} \\ &= \frac{|\mathbb{B}(\mathbf{k},\mathbf{k_0})|^2}{\kappa Q_z^2}\int_{\mathbf{r}} e^{-j\mathbf{Q_H}\cdot\mathbf{r}}\left[e^{-\frac{1}{2}Q_z^2\mathcal{D}(\mathbf{r})}-e^{-Q_z^2\sigma_\eta^2}\right]d\mathbf{r},\end{aligned} \tag{29}$$

with σ_η^2 the height mean square value, W the height autocorrelation function and $\mathcal{D}$ the height structure function defined as

$$\mathcal{D}(\mathbf{r}) = 2\left[\sigma_\eta^2 - W(\mathbf{r})\right]. \tag{30}$$

TABLE II
SIMULATION PARAMETERS

Frequency f	10 GHz
Radar wavelength λ_0	0.03 m
Number of samples N	2^{13}
Sampling interval Δ	$\lambda_0/10$
Wind speed u_{10}	8 m/s

So, the BNRCS is directly linked to the Fourier transform of a function $\mathcal{F}$ which is related to the sea surface characteristics,

$$\mathcal{F}(\mathbf{r}) = e^{-\frac{1}{2}Q_z^2 \mathcal{D}(\mathbf{r})}. \tag{31}$$

Then, by applying the SDM and studying the function $\mathcal{F}$, one can ensure a correct estimation of the BNRCS.

IV. GENERATED SURFACE CHARACTERISTICS

It is necessary to analyze the generated surface characteristics to check its realism in comparison to that obtained from the conventional method. First, the interpolation process impact (for LF sea surface generation) on sea surface height spectrum is investigated. Secondly, the generated surface characteristics from combination techniques (for HF sea surface generation) introduced in subsection II-C are studied. For a sake of clarity, this study is conducted for 2D problems but the results can be extended to 3D problems.

A. Interpolation Techniques

One scenario is proposed here and the parameters are listed in Tab. II. Before the interpolation process, the cutoff-wavenumber k_c is $\pi/(P\Delta)$; after, it becomes equal to π/Δ with $P = 8$ the interpolation parameter. Fig. 5 illustrates the isotropic part of sea surface height spectrum from the model of Elfouhaily et al. [6] versus the wavenumber k. Three interpolation techniques are studied: linear, quadratic and cubic. The full sea surface height spectrum is obtained by both a numerical computation ($S_{\mathrm{LF}}(k)$ Num) –which consists in a Monte-Carlo process by generating 500 sea surfaces and then by computing their sea surface height spectrum– and the analytical expression [6] ($S_{\mathrm{LF}}(k)$ Theory). First, one can observe that interpolation processes create higher frequency harmonics than the original generation. Also, it can be seen that the quadratic interpolation presents over-occurred harmonics which can severely disturb the BNRCS, especially by using the Small Perturbation Method (SPM), that is directly proportional to high-frequencies sea surface height spectrum. Besides, linear and cubic interpolations seem to be relevant techniques to upgrade the sampling intervals of a given sea surface, creating low energy high frequency components. So, linear interpolation is the best choice by adding time and/or computer resources optimizations. Fig. 6 plots the isotropic part of interpolated sea surface height spectrum versus the wavenumber k. The wind speed u_{10} is 8 m/s. The linear interpolation method is considered. Three values of the interpolation parameter are studied: 8, 16 and 32. This result shows a qualitatively-low impact of the interpolation parameter and has to be

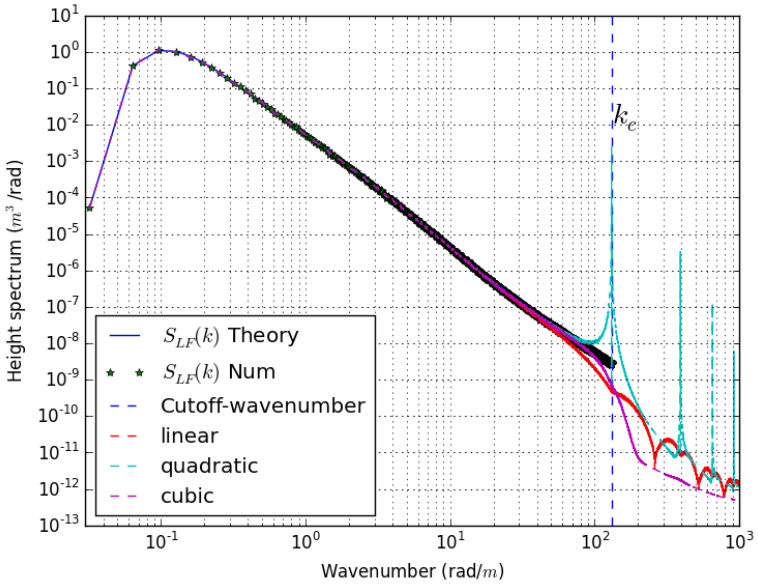

Fig. 5. Isotropic part of the sea surface height spectrum S_{LF} versus the surface wavenumber k from the model of Elfouhaily et al. [6]. Wind speed is $u_{10} = 8$ m/s. Both the numerical and theoretical spectra S_{LF} –with and without sea surface generation– are presented. The cutoff-wavenumber before the interpolation process $k_c = 131$ rad/m is also displayed. Three interpolation techniques are illustrated, linear, quadratic and cubic.

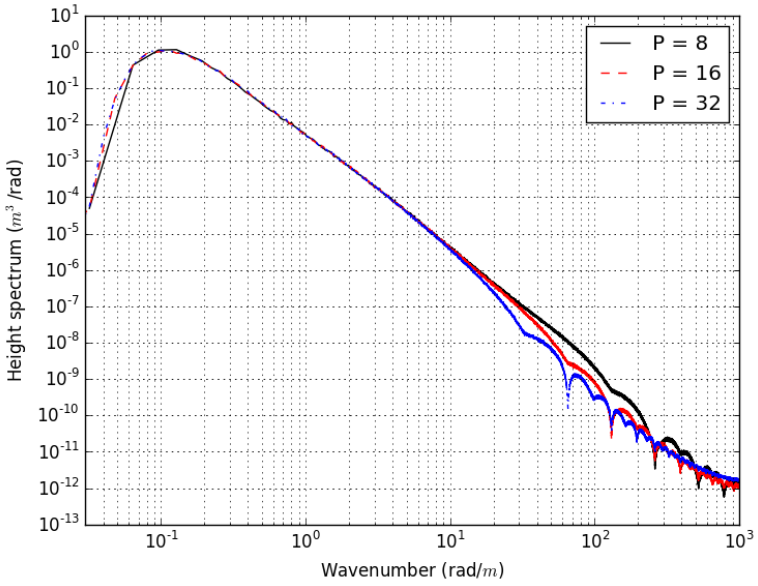

Fig. 6. Isotropic part of the interpolated sea surface height spectrum versus the surface wavenumber k from the model of Elfouhaily et al. [6]. Wind speed is $u_{10} = 8$ m/s. Three interpolation parameters are presented, $P = \{8; 16; 32\}$, the interpolation method is linear.

discussed after adding the HF surface. Moreover, an interpolation process –especially when linear– is efficient to reduce the sampling interval at almost no added cost. Besides, the more the interpolation parameter P is, the earlier the oscillations occur in the sea surface height spectrum. This phenomenon is explained by the chosen sampling

interval to reach. Indeed, before the interpolation process, the maximum wavenumber value is $k_{\max}=\pi/(P\Delta)$, so, the more the interpolation parameter P is, the shorter $k_{\max}$ is and thus, the earlier the oscillations occur.

B. Combination Techniques

The scenario is similar to that one in subsection IV-A, Tab. II. While, P surfaces are now combined thanks to one of those techniques presented in subsection II-C. Before the combination process, the HF surface length L is $N\times\Delta$ and after, it will be $P\times L$ with P the number of combined surfaces. Thus, the cutoff-wavenumber before the combination technique is $k_{\min}=2\pi/L$. Fig. 7 plots the isotropic part of sea surface height spectrum versus the surface wavenumber. This spectrum is compared to those performed by using a combination technique. Fig. 7a illustrates the RST, the theoretical spectrum of RST previously derived in Eq. (16) is also displayed and is in accordance with the numerical one. The RST slightly overestimates the harmonics within the spectrum. Despite the apparition of harmonics lower than that located in $k_{\min}$, the CST seems to get the best accuracy by ensuring continuity and preserving from overestimated harmonics, Fig. 7b. Moreover, the SDM height mean square value ($\sigma^2_{\text{HF, X}}$, X the combination technique) is in accordance with the conventional one (σ^2_{HF}). Indeed, $\sigma^2_{\text{HF}}=0.084$ m^2, $\sigma^2_{\text{HF, RST}}=0.086$ m^2 and $\sigma^2_{\text{HF, CST}}=0.083$ m^2. Fig. 8 plots the combined sea surfaces height spectrum versus the surface wavenumber k by using the CST. Whatever the number P of combined surfaces is (between 8 and 32), the height spectrum is qualitatively similar.

C. Height Spectrum and Height Structure Function

The SDM is applied to create a $N\times P$-samples sea surface with a sampling interval Δ. Firstly, one sea surface with N samples and a sampling interval $P\times\Delta$ is generated and then linearly interpolated to get a new sampling interval Δ. Secondly, one sea surface with N samples and a sampling interval Δ is generated to perform RST and CST and therefore, to create a combinated sea surface with $N\times P$ samples and a sampling interval Δ. Then, these two surfaces are added to generate the composite two-scales surface. Notice that, to avoid spectral redundancy between the two spectra used to generate these two surfaces, harmonics in the interval I are forced to 0 in the first spectrum –that is the LF part– with

$$I=\left[\frac{2\pi}{N\Delta},\frac{\pi}{P\Delta}\right]. \tag{32}$$

The frequency is 10 GHz, $N=2^{13}$ samples, $\Delta=\lambda_0/10$ with λ_0 the wavelength, $P=8$ and the wind speed u_{10} is 8 m/s. This generation is repeated over a Monte-Carlo process by generating 500 composite two-scales sea surfaces. Fig. 9 plots the isotropic part of sea surface height spectrum versus the surface wavenumber. This spectrum is compared to those performed by using the SDM. Once again, harmonics lower than that located in $k_c=2\pi/(N\Delta)$ are greater than their theoretical counterparts in CST, Fig. 9b. Indeed, this technique is based on the combination of independent surfaces. Fig. 9a illustrates the RST. As previously depicted in Fig. 7, the latter overestimates the harmonics within the spectrum. Finally and again, the CST gets the best accuracy by ensuring continuity and preserving from overestimated harmonics. After a spectral investigation of SDM, a spatial analysis is necessary through the heigh structure function introduced in Eq. (30). Indeed, this quantity leads to the BNRCS

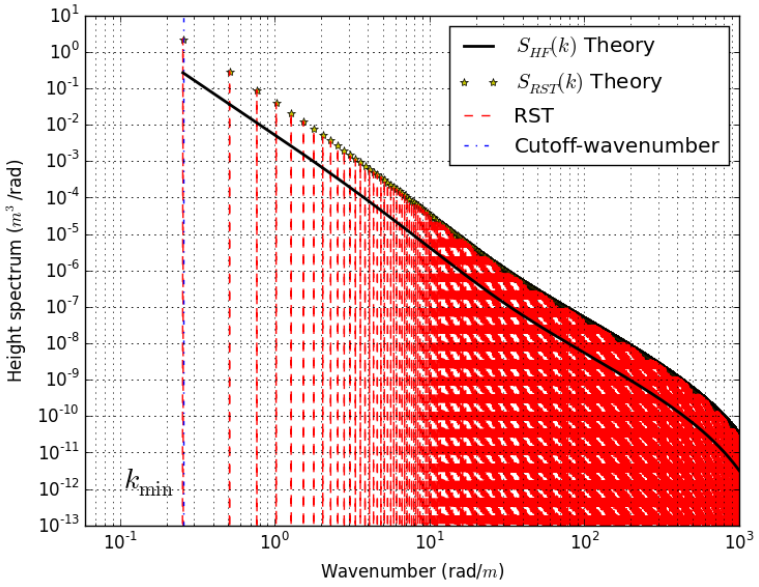

(a) Repeated Surfaces Technique

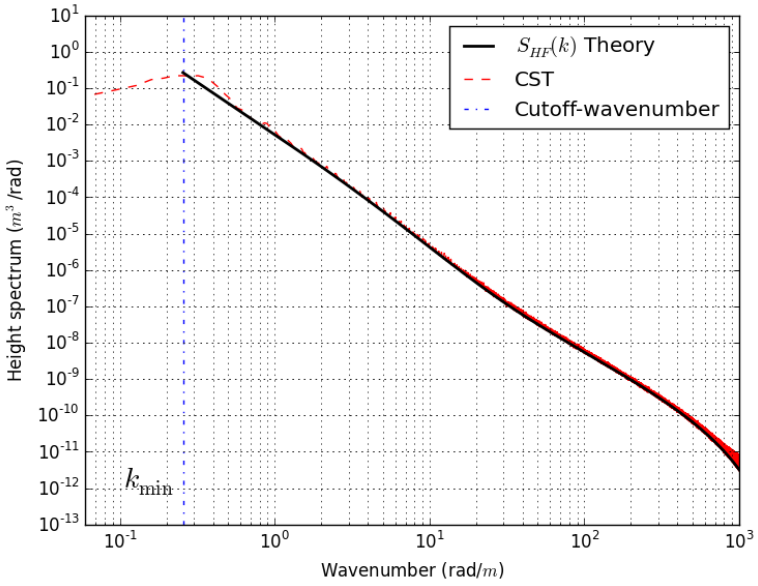

(b) Combined Surfaces Technique

Fig. 7. Isotropic part of the sea surface height spectrum S_{HF} versus the surface wavenumber k from the model of Elfouhaily et al. [6]. Wind speed is $u_{10} = 8$ m/s. The cutoff-wavenumber before the combination process $k_{\min}$ is also displayed. The isotropic part of the sea surface height spectrum from the two combination techniques introduced in subsection II-C are also illustrated; RST (7a) and CST (7b).

estimation by using SSA1 (Eq. (29)). Fig. 10 plots the theoretical height structure function ($\mathcal{D}(x)$ Theory) versus the surface position. This height structure function is compared to the two obtained thanks to SDM. The RST produces oscillations within the height structure function. This phenomenon is produced by the repetition process and so, by the correlation renewal between one surface elevation point and its copy, located every $N \times \Delta$ meters. The CST height structure function is qualitatively in accordance with the theoretical one.

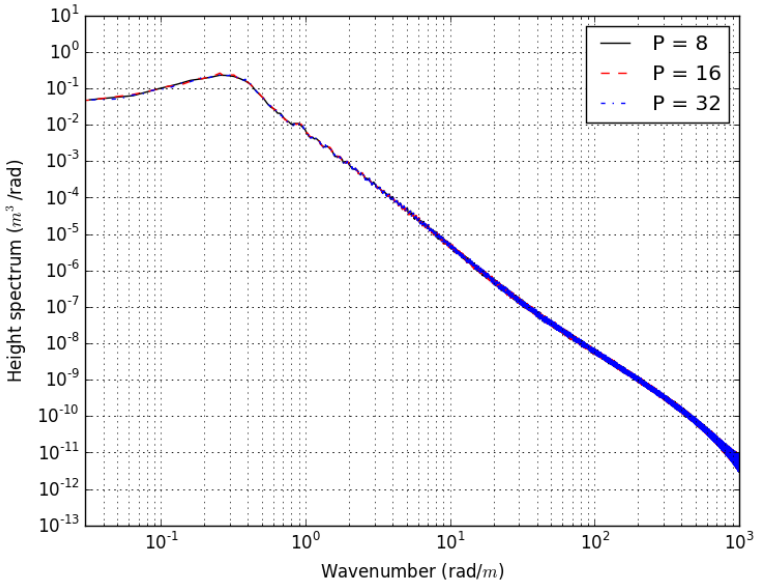

Fig. 8. Isotropic part of the combined sea surfaces height spectrum versus the surface wavenumber k from the model of Elfouhaily et al. [6]. Wind speed is $u_{10} = 8$ m/s. The inspected combination technique is the CST. Three parameters are shown; 8, 16 and 32.

D. From sea surface characteristics to BNRCS

The right description of the function $\mathcal{F}$ defined in Eq. (31) is a crucial step into the BNRCS computation. Indeed, as previously described, this function is one of the key-parameter in the analytical expression of the BNRCS with SSA1 Eq. (29). Therefore, by ensuring a non-impact of combination techniques on this function, SDM becomes a relevant way to compute the BNRCS from sea surfaces. Fig. 11 plots the theoretical $\mathcal{F}$ function versus the surface position. Those computed by using SDM and the two different combination techniques, RST and CST, are also displayed. Two incidence angles are considered here, $\theta = 0°$, which is located in the Geometrical Optics domain, and $\theta = 60°$ in the Bragg scattering domain. Whatever the combination technique is, the SDM is in accordance with the theory and so, will not disturb the BNRCS estimation.

V. Sea Surface BNRCS

A two-dimensional problem is considered to compute the sea surface BNRCS. The same parameters introduced in Tab. II are chosen and the SDM parameter P (that is the number of combined surfaces) is 8. The sea surface BNRCS is computed with a monostatic configuration and HH polarization. The sea dielectric permittivity ε is $53.2 + j37.8$. To obtain this BNRCS, a thousand of sea surfaces are generated. Thus, the surface length is $N \times P \times \Delta \approx 196$ m and the gravity waves are correctly taken into account in the sea surface height spectrum, Eq. (26). For this scenario, we study the impact induced by the combination technique –and therefore the SDM– on the sea surface BNRCS. Fig. 12a and 12b plot the incoherent monostatic BNRCS versus the incidence angle from a conventional sea surface generation –spectral method introduced in subsection II-A– and from SDM with either RST or CST. The ratios between RST / CST and the reference are also showed in Fig. 12c and 12d. One can see that the SDM and any

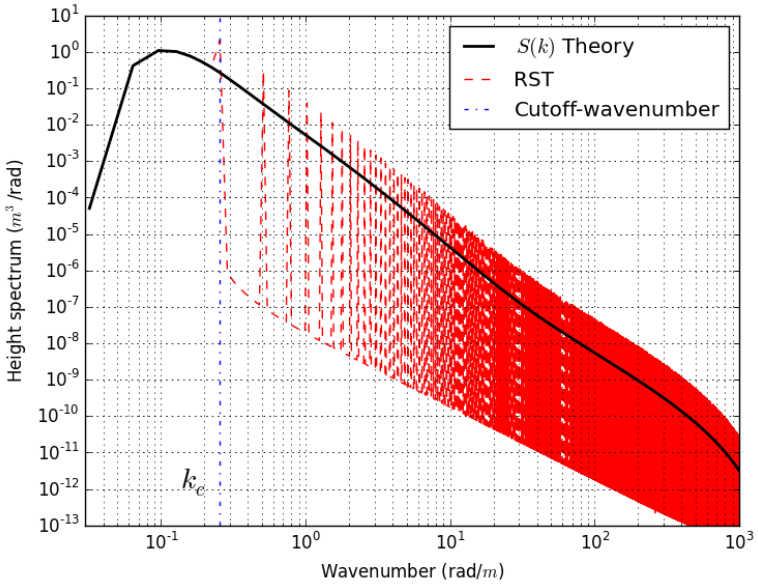

(a) Repeated Surfaces Technique

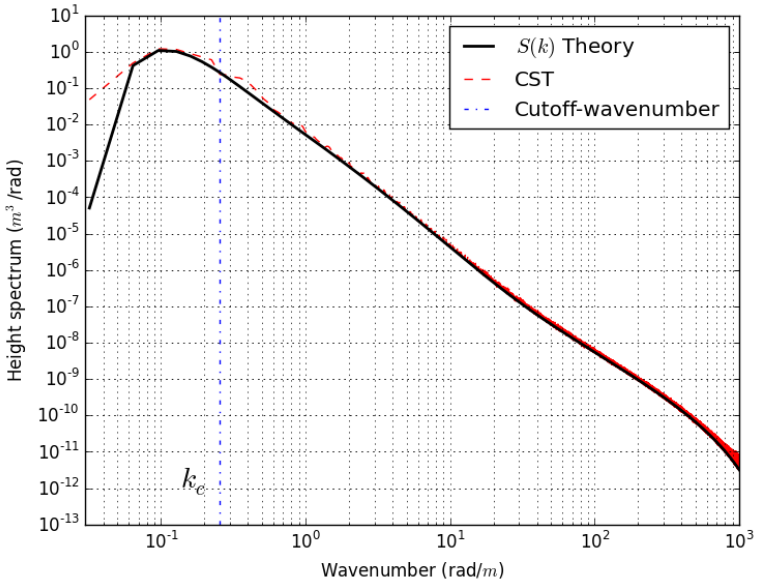

(b) Combined Surfaces Technique

Fig. 9. Isotropic part of the sea surface height spectrum $S(k)$ versus the surface wavenumber k from the model of Elfouhaily et al. [6]. Wind speed is $u_{10}=8$ m/s. The isotropic part of the sea surface height spectrum from the two combination techniques introduced in subsection II-C are also illustrated; RST (9a) and CST (9b).

of the suggested combination techniques do not quantitatively disturb the BNRCS estimation, both in VV and HH polarizations. For RST, the maximal error is ± 1 dB and for CST, the error is about 0 dB after the incidence angle 15° and remains inferior to ± 1 dB along the incidence angle track. The error function is similar whatever the polarization is. Indeed, only the sea surface generation process is modified and this does not impact on the polarization term within SSA1, Eq. (27). Thus, SDM with RST is an efficient mean to perform numerical computation of the sea

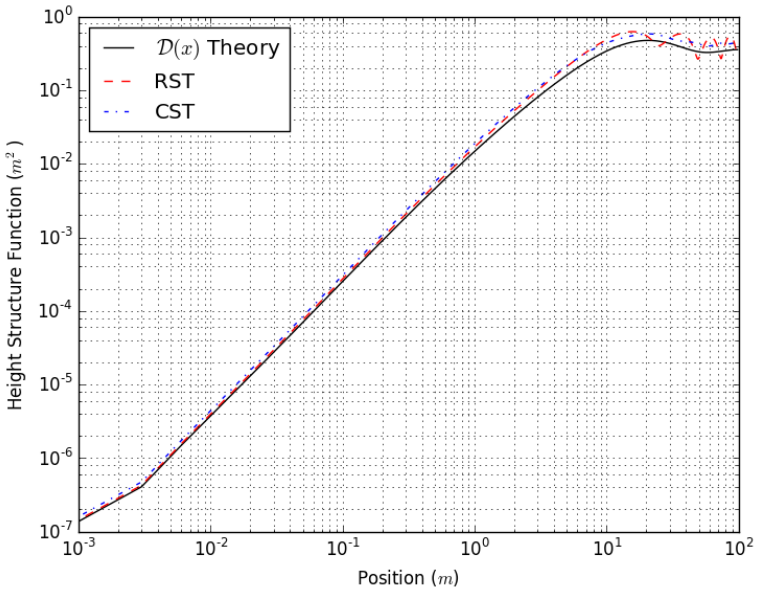

Fig. 10. Height structure function $\mathcal{D}$ versus the surface position x from the model of Elfouhaily et al. [6]. Wind speed is $u_{10} = 8$ m/s. The theoretical height structure function $\mathcal{D}$ is plotted in full black line. The two combination techniques from subsection II-C are illustrated in dashed-red and discontinuous-blue line; RST and CST respectively.

surface BNRCS. Then, the effect of the parameter P is investigated. Three values are chosen, $P = \{8, 16, 32\}$. To keep the same sea surface length, the number of samples N is modified in consequence and the sampling interval is kept constant, $\Delta = \lambda_0/10$, as previously stated. The two polarizations VV and HH are studied. Fig. 13a and 13b plot the incoherent monostatic BNRCS in VV or HH polarization versus the incidence angle from SDM with either RST or CST and by applying different P parameters. The two combination techniques are discriminated thanks to an offset (-10 dB for CST). The results show a same trend for VV or HH polarization, the tested parameter P values have no impact on the result. This observation is confirmed by Fig. 13c and 13d. Indeed, the BNRCS ratio between $P = \{16, 32\}$ and $P = 8$ is inferior to ± 1 dB along the incidence angle track, and so, whatever the investigated combination technique is. Again, the two combination techniques are discriminated thanks to an offset (-2 dB for CST). Like in Fig.12c and 12d, these error functions are similar; the sea surface generation process does not interfere with the polarization term in SSA1, Eq. (27).

VI. Summary and Outlooks

Sea surface generation is a high-demanding process to achieve accurate BNRCS. Indeed, large sea surface areas and high resolution are required. In this context, the Spectral Decomposition Method (SDM) is a relevant tool to make the sea surface generation faster. The former is formalized and the new sea surface generation process is introduced. An interpolation and a combination technique are necessary to complete this generation. Three kinds of interpolation are suggested, namely, linear, quadratic and cubic. Two combination techniques are also investigated, the Repeated Surfaces Technique (RST) and the Combined Surfaces Technique (CST). Then, the SDM computational complexity is compared to the reference one, it appears that the SDM reduces the complexity by a factor between 10

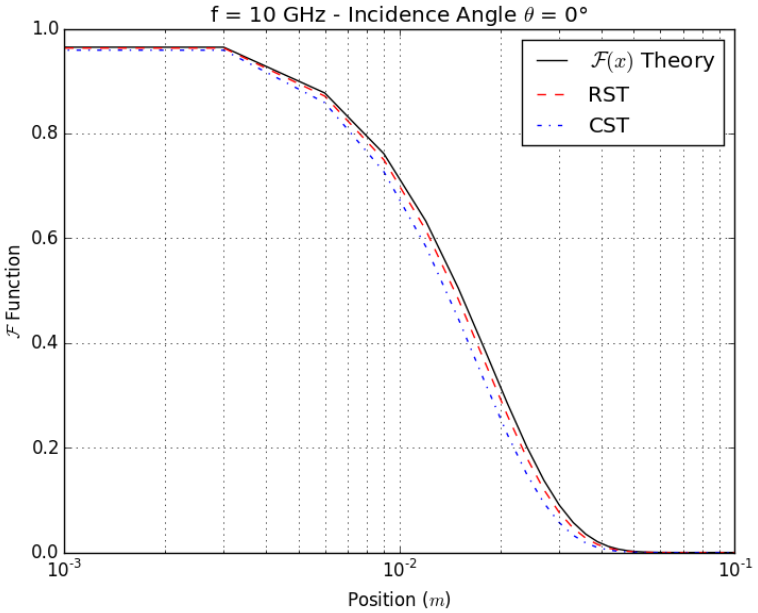

(a) Incidence Angle 0°

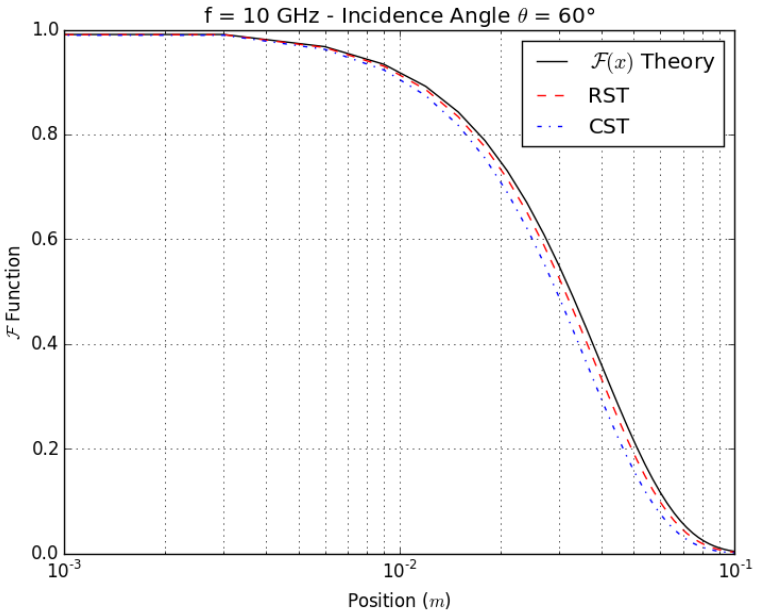

(b) Incidence Angle 60°

Fig. 11. $\mathcal{F}$ function versus the surface position x from the model of Elfouhaily et al. [6]. Wind speed is $u_{10} = 8$ m/s for a frequency $f = 10$ GHz. The theoretical $\mathcal{F}$ function is plotted. The two combination techniques from subsection II-C are illustrated; RST and CST.

and 200, depending on the chosen combination technique. Similarly, the memory consumption is drastically reduced by using SDM rather than a conventional method, the ratio is roughly from 10^{-2} to 10^{-3}. The SDM and these interpolation and combination techniques are studied through the generated sea surface characteristics and through the sea surface BNRCS. About the interpolation process, the linear method is the best choice. Indeed, the linear

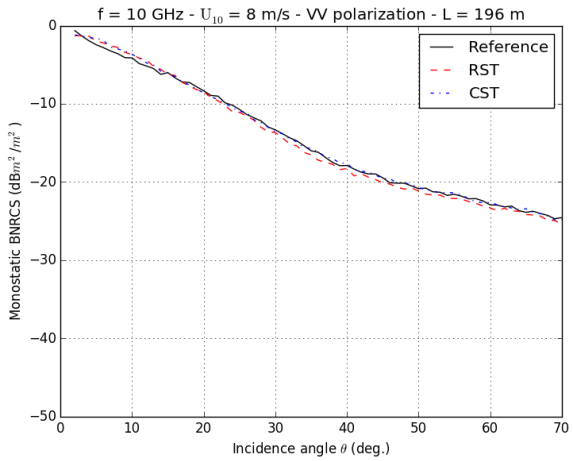

(a) Incoherent monostatic BNRCS versus the incidence angle, VV polarization

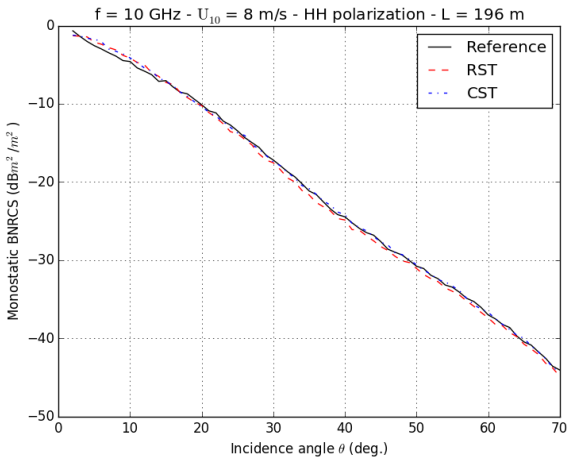

(b) Incoherent monostatic BNRCS versus the incidence angle, HH polarization

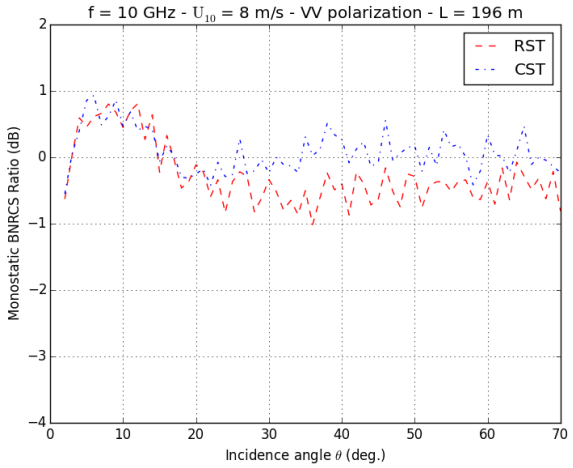

(c) Incoherent monostatic BNRCS ratio versus the incidence angle, VV polarization

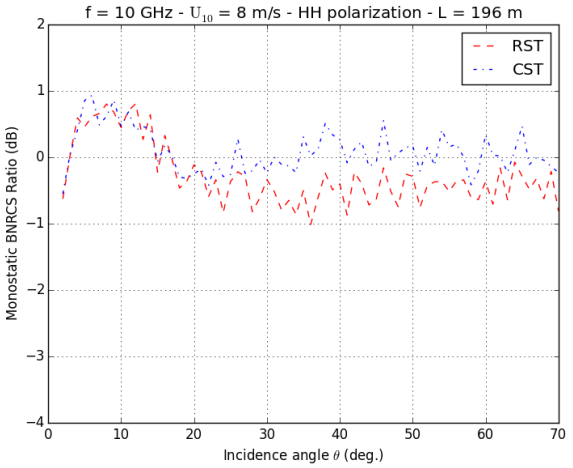

(d) Incoherent monostatic BNRCS ratio versus the incidence angle, HH polarization

Fig. 12. The wind speed is 8 m/s for a frequency $f = 10$ GHz in VV and HH polarizations. Comparison of the SSA1 from conventional sea surface generation and the SSA1 from SDM, considering the two different combination techniques. 1000 surfaces of length $L = 196$ m were generated.

method is the quickest interpolation process and presents weak distortions within the sea surface height spectrum (crucial parameter since its inverse Fourier transform drives sea surface NRCS from SSA1). Besides, despite different behaviours linked to each of the proposed combination techniques on the sea surface height spectrum and on the height structure function, the sea surface BNRCS computed from the SDM with either the RST or the CST is in agreement with the one from a conventional sea surface generation. Therefore, the SDM is valid from near nadir sensors like altimeters to moderate observation angles. This approach is analytically formalized –both in spatial and frequency domains for RST– and tested for a subdivision in two spectra according to the sea surface characteristics and the BNRCS.

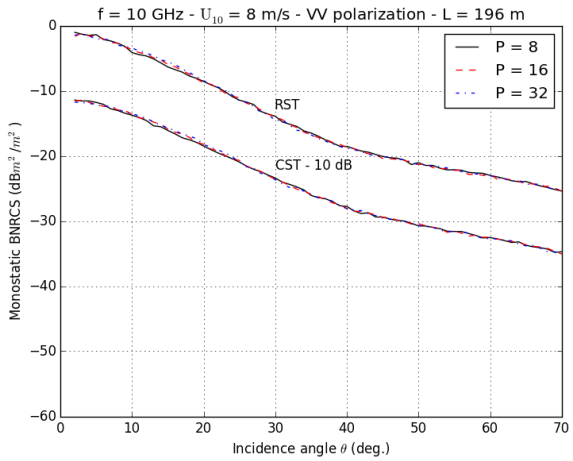

(a) Incoherent monostatic BNRCS versus the incidence angle, VV polarization, RST and CST - 10 dB

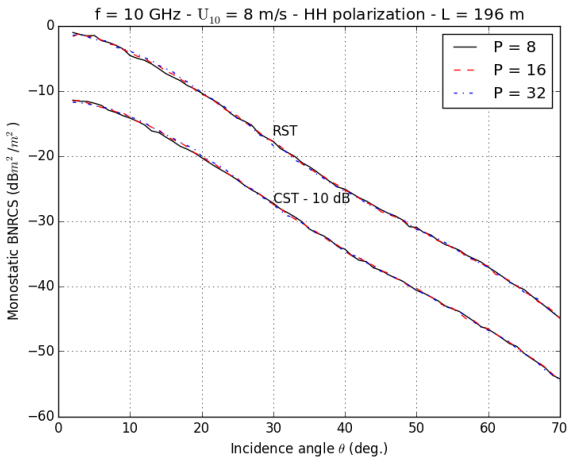

(b) Incoherent monostatic BNRCS versus the incidence angle, HH polarization, RST and CST - 10 dB

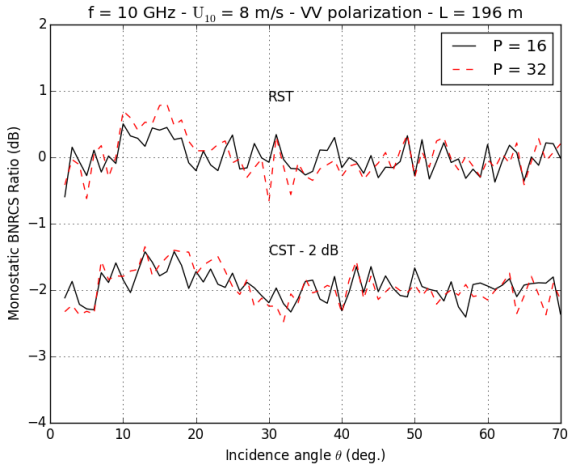

(c) Incoherent monostatic BNRCS ratio versus the incidence angle, VV polarization, RST and CST - 2 dB

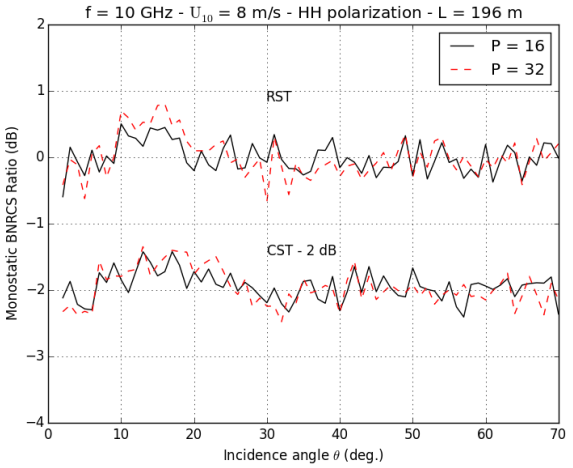

(d) Incoherent monostatic BNRCS ratio versus the incidence angle, HH polarization, RST and CST - 2 dB

Fig. 13. The wind speed is 8 m/s for a frequency $f = 10$ GHz in VV and HH polarizations. Comparison of the SSA1 with different P parameters and considering the two combination techniques. 1000 surfaces of length $L = 196$ m were generated. CST - X dB stands for an offset of X dB to improve the discrimination between the two techniques.

This process is a relevant tool to accelerate the radar backscattering computation from large sea surfaces. In future work, it should be coupled with a two-scale electromagnetic model to further speed up the simulation. Moreover, the spectral decomposition method could be used to simulate sea surfaces with range variations of characteristics (wind speed in particular) and then compute composite sea surfaces, closer to the real weather conditions.

APPENDIX A
RST SEA SURFACE HEIGHT SPECTRUM

From Eq. (10),

$$h_{\text{HF,RST}}(x) = h_{\text{HF}}(x) * \sum_{n=0}^{P-1} \delta(x - nL) = \sum_{n=0}^{P-1} h_{\text{HF}}(x - nL), \tag{33}$$

with h_{HF} the P-times-repeated surface, L its length, $h_{\text{HF,RST}}$ the composed surface of length $P \times L$ and δ the Dirac delta function. Then, the height autocorrelation function $W_{\text{HF,RST}}$ from RST is expressed as

$$\begin{aligned} &W_{\text{HF,RST}}(r) = \\ &\frac{1}{P} \sum_{n=0}^{P-1} \sum_{m=0}^{P-1} \langle h_{\text{HF}}(x_1 - nL) h^*_{\text{HF}}(x_1 + r - mL) \rangle \\ &= \frac{1}{P} \sum_{n=0}^{P-1} \sum_{m=0}^{P-1} \langle h_{\text{HF}}(\alpha_n) h^*_{\text{HF}}(\alpha_n + r + (n-m)L) \rangle \\ &= \frac{1}{P} \sum_{n=0}^{P-1} \sum_{m=0}^{P-1} W_{\text{HF}}(r + (n-m)L), \end{aligned} \tag{34}$$

with W_{HF} the theoretical height autocorrelation function, x_1 an abscissa and $\alpha_n = x_1 - nL$. Therefore, by taking the Fourier transform of the height autocorrelation function, one can get

$$S_{\text{HF,RST}}(k) = \frac{S_{\text{HF}}(k)}{P} \sum_{n=0}^{P-1} \sum_{m=0}^{P-1} \exp[jk(n-m)L]. \tag{35}$$

Furthermore,

$$\begin{aligned} &\sum_{n=0}^{P-1} \sum_{m=0}^{P-1} \exp[jk(n-m)L] = \\ &\qquad \left[\sum_{n=0}^{P-1} \exp(jknL) \right] \left[\sum_{m=0}^{P-1} \exp(jkmL) \right]^*. \end{aligned} \tag{36}$$

This expression can be simplified by using formulae from geometric series to finally obtain

$$S_{\text{HF,RST}}(k) = \frac{1}{P} \left| \frac{\sin(\frac{kPL}{2})}{\sin(\frac{kL}{2})} \right|^2 S_{\text{HF}}(k), \tag{37}$$

with $S_{\text{HF}}(k)$ the theoretical sea height spectrum. That is the response of a uniform linear array of phased array antenna with S_{HF} the elementary antenna.

ACKNOWLEDGMENT

The authors would like to thank Total company for the fundings and especially Veronique Miegebielle and Philippe Lattes for supporting this work.

REFERENCES

[1] A. G. Voronovich, "Small-slope approximation in wave scattering by rough surfaces," *Journal of Experimental and Theoretical Physics*, vol. 62, pp. 65–70, 1986.

[2] N. Pinel, G. Monnier, J. Houssay, and A. Becquerel, "Fast simulation of a moving sea surface remotely sensed by radar," in *International Radar Conference, 2014*. IEEE, 2014.

[3] W. Jiang, M. Zhang, P.-B. Wei, and D. Nie, "Spectral Decomposition Modeling Method and Its Application to EM Scattering Calculation of Large Rough Surface With SSA Method," *Journal of Selected Topics in Applied Earth Observations and Remote Sensing*, vol. 8, no. 4, pp. 1848–1854, 2015.

[4] W. Jiang, M. Zhang, Y. Zhao, and D. Nie, "EM scattering calculation of large sea surface with SSA method at S , X , Ku , and K bands," *Waves in Random and Complex Media*, 2016. [Online]. Available: http://dx.doi.org/10.1080/17455030.2016.1213463

[5] L. Tsang, J. Au Kong, K.-H. Ding, and C. O. Ao, *Scattering of Electromagnetic Waves: Numerical Simulations*, J. Au Kong, Ed. John Wiley & Sons, Inc., 2002.

[6] T. M. Elfouhaily, B. Chapron, K. Katsaros, and D. Vandemark, "A unified directional spectrum for long and short wind-driven waves," *Journal of Geophysical Research: Oceans*, vol. 102, pp. 15 781–15 796, 1997. [Online]. Available: http://doi.wiley.com/10.1029/97JC00467

[7] N. Jeannin, L. Féral, H. Sauvageot, L. Castanet, and F. Lacoste, "A Large-Scale Space-Time Stochastic Simulation Tool of Rain Attenuation for the Design and Optimization of Adaptive Satellite Communication Systems Operating between 10 and 50 GHz," *International Journal of Antennas and Propagation*, 2012.

[8] N. Pinel and C. Bourlier, *Electromagnetic Wave Scattering from Random Rough Surfaces: Asymptotic Models*. Hoboken, USA: John Wiley & Sons, Inc., 2013. [Online]. Available: http://doi.wiley.com/10.1002/9781118579152

[9] C. Bourlier, N. Pinel, and G. Kubicke, *Method of Moments for 2D Scattering Problems: Basic Concepts and Applications*. Hoboken, USA: John Wiley & Sons, Inc., 2013.

[10] C. Bourlier, N. Déchamps, and G. Berginc, "Comparison of asymptotic backscattering models (SSA, WCA, and LCA) from one-dimensional Gaussian ocean-like surfaces," *IEEE Transactions on Antennas and Propagation*, vol. 53, no. 5, pp. 1640–1652, 2005.